Applied Physics Letters

Controlling avalanche soliton nucleation in a chiral soliton lattice on a monoaxial chiral magnet $CrNb_3S_6$ by dynamic strain

Cite as: Appl. Phys. Lett. **118**, 132404 (2021); https://doi.org/10.1063/5.0040327
Submitted: 11 December 2020 . Accepted: 12 March 2021 . Published Online: 30 March 2021

M. Ohkuma, M. Mito, Y. Kousaka, J. Akimitsu, J. Kishine, and K. Inoue

Applied Physics Letters ARTICLE scitation.org/journal/apl

Controlling avalanche soliton nucleation in a chiral soliton lattice on a monoaxial chiral magnet $CrNb_3S_6$ by dynamic strain

Cite as: Appl. Phys. Lett. **118**, 132404 (2021); doi: 10.1063/5.0040327
Submitted: 11 December 2020 · Accepted: 12 March 2021 ·
Published Online: 30 March 2021

View Online Export Citation CrossMark

M. Ohkuma,[1,a)] M. Mito,[1,2] Y. Kousaka,[2,3] J. Akimitsu,[2,4] J. Kishine,[2,5,6] and K. Inoue[2,7,8]

AFFILIATIONS

[1]Graduate School of Engineering, Kyushu Institute of Technology, Kitakyushu 804-8550, Japan
[2]Chirality Research Center, Hiroshima University, Higashihiroshima 739-8526, Japan
[3]Department of Physics and Electronics, Osaka Prefecture University, 1-1 Gakuencho, Sakai, Osaka 599-8531, Japan
[4]Research Institute for Interdisciplinary Science, Okayama University, Okayama 700-8530, Japan
[5]Division of Natural and Environmental Sciences, The Open University of Japan, Chiba 261-8586, Japan
[6]Institute for Molecular Science, 38 Nishigo-Naka, Myodaiji, Okazaki, 444-8585, Japan
[7]Graduate School of Advanced Science and Engineering, Hiroshima University, Higashihiroshima 739-8526, Japan
[8]Institute for Advanced Materials Research, Hiroshima University, Higashihiroshima 739-8526, Japan

[a)]**Author to whom correspondence should be addressed:** m108022m@mail.kyutech.jp

ABSTRACT

The monoaxial chiral magnet $CrNb_3S_6$ exhibits a chiral soliton lattice (CSL) upon application of an external magnetic field (H) perpendicular to the helical axis (c-axis). The increase in the soliton (kink) number of the CSL in the process of decreasing H accompanies soliton penetration after nucleation at the surface. Avalanche soliton nucleation occurs during the initial process of soliton nucleation. We applied dynamic strain with scores of MHz to the crystal with the crystal size along the c-axis of 10 μm from the edge of the c-axis, so that we controlled the avalanche soliton nucleation by modifying the surface barrier. The present results suggest that the acoustic wave is useful for controlling the soliton number.

Dzyaloshinskii–Moriya (D–M) interaction stabilizes a chiral helimagnetic structure in non-centrosymmetric bulk magnets.[1,2] In the case of a monoaxial D–M interaction, a chiral soliton lattice (CSL), which is stabilized by applying a magnetic field (H) perpendicular to the helical axis, shows peculiar transport and magnetic properties accompanying the change in the number of magnetic kinks termed solitons of the CSL.[3,4] Solitons nucleated at the surface penetrate into the interior of the crystal, and annihilation of the solitons occurs after movement to the surfaces.[5,6] A crystal surface deeply connected to the topological stability plays an important role in the nucleation and annihilation of solitons.

Experimentally, the CSL was first observed in the monoaxial chiral magnet $CrNb_3S_6$ through Lorentz transmission electron microscopy (TEM).[7] Figure 1(a) illustrates the changes in the magnetic configuration along the chiral helix as a function of H: At $H = 0$, and a helimagnetic structure whose helical pitch is 48 nm appears along the c-axis below the transition temperature ($T_c = 127$ K).[7,8] By applying H perpendicular to the c-axis, the CSL is stabilized and turns into a forced ferromagnetic (FFM) state for H greater than the critical magnetic field (H_c). In $CrNb_3S_6$, discrete changes in magnetization (M) and magnetoresistance (MR) have been observed during the H-decreasing process, especially in the boundary between the FFM and CSL states.[5,6,9–14] These phenomena can be explained by the surface barrier due to surface twists.[6,15–18] Noticeable discrete changes in M and MR reflect avalanche soliton nucleation, and the discreteness is related to the magnitude of the surface barrier.

The effects of static structural modifications on $CrNb_3S_6$ have been investigated. In combination with the structural analysis and magnetic measurements under high pressure, it was suggested that the change in the structural symmetry of the CrS_6 octahedron affected the exchange network between magnetic Cr^{3+} ions and the D–M interaction.[19] The effects of uniaxial elastic strain perpendicular to the chiral

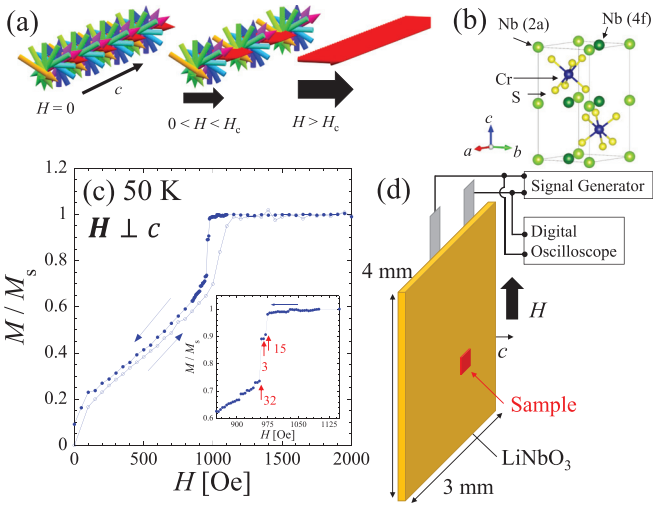

FIG. 1. (a) Magnetic structure of monoaxial chiral magnets under the magnetic field (H), helimagnetic state (left, at $H = 0$), chiral soliton lattice (CSL) (center, $0 < H < H_c$), and forced ferromagnetic (FFM) state (right, $H > H_c$). (b) Crystal structure of $CrNb_3S_6$. (c) M–H curve of a single crystal of $CrNb_3S_6$ at 50 K. The inset shows discrete changes between the FFM state and the CSL during the H-decreasing process. Numbers indicate the number of changes in solitons, estimated based on discrete changes in M. (d) Overview of the experimental setup. The sample was bonded to the $LiNbO_3$ transducer coated with gold with a vulcanized rubber.

axis of the thin film of $CrNb_3S_6$ have been studied through the Lorentz TEM experiments.[20] Non-trivial topological spin textures described by the double sine-Gordon model were stabilized by strain-induced anisotropies.[20] Thus, uniaxial and hydrostatic structural modifications are useful methods for manipulating spin texture of monoaxial chiral magnets. Recently, the magneto-structural correlation has been observed in the form of magnetostriction.[21]

Some of the authors previously reported the effects of dynamic strain on a thin film (10 μm along the c-axis, $5 \times 0.5\ \mu m^2$; the maximum soliton number is approximately 209) of $CrNb_3S_6$ by measuring MR at 100 and 110 K.[22] In the previous study, they demonstrated that they changed the FFM state to the CSL state by using a piezoelectric transducer that produced the expanding mode type of acoustic wave with a characteristic frequency of 1 MHz. The acoustic wave was not directional with regard to the chiral axis. In the process of decreasing H starting from the FFM state, a continuous application of dynamic strain disturbed the soliton nucleation. In contrast, a pulse-type dynamic strain application just before avalanche soliton nucleation induced the soliton nucleation. However, the magnitude of avalanche soliton nucleation, that is, the number of solitons in avalanche soliton nucleation, was not controlled. There, various discrete chiral magnetic soliton states were not created by dynamic strain.

In this Letter, we investigated the possibility of controlling the avalanche soliton nucleation by dynamic strain at lower temperatures. We used a single crystal that had submillimeter scale on the surface area of the ab-plane (S_{ab}) and micrometer scale on the crystal size along c-axis (L_c), which was the same dimension as in Ref. 14. Figure 1(c) shows the M–H curve of the crystal at 50 K. The M–H curves in the H-decreasing process showed several discrete changes. This crystal is suitable for observing the change in M due to the avalanche soliton nucleation by dynamic strain. We changed the number of solitons in the CSL and the magnetic configuration from the FFM state to the CSL by using dynamic strain.

A single crystal of $CrNb_3S_6$ was synthesized using a chemical transport method, whereby the details of the synthesis are described elsewhere.[23] S_{ab} and L_c were approximately 0.375 mm^2 and 75 μm, respectively. We reduced the crystal size down to approximately 0.055 mm^2 on S_{ab} and 10 μm on L_c (permitting approximately 209 solitons) by using a method reported previously.[14] M measurements were performed using a commercial superconducting quantum interference device (SQUID) magnetometer (Quantum Design Ltd.). The sample was bonded to the $LiNbO_3$ transducer coated with gold with a vulcanized rubber. The ab-plane of the sample was parallel to the plane of the transducers, as shown in Fig. 1(d). We used the transverse type transducer with a characteristic frequency of approximately 17 MHz. The sinusoidal voltage was applied to the transducer by using signal generators (NF Corporation, WF1947 for Fig. 2, Rohde & Schwarz, SMB100A for Fig. 3). The magnitude of the vibration depends on the voltage V applied to both electrodes of the transducers. In order to avoid heating effects as much as possible, we controlled the time of voltage application to less than 300 ms. H was applied perpendicular to the c-axis. In order to focus the soliton nucleation after overcoming a certain surface barrier, we measured the M–H curve in the process of decreasing H starting from the FFM state. The M measurements were performed four times after stabilizing each H and/or applying a pulse-like voltage to the transducers. The data shown in this study are the average of the latter three of the four measurements, with the exception of the first dataset, to investigate the equilibrium state. The diamagnetic background due to $LiNbO_3$ was subtracted from the data.

Figure 2 shows M during the H-decreasing process from 2000 Oe ($>H_c$) at 50 K. We measured M in intervals of 5 Oe around the boundary between the FFM and CSL states, and M was normalized with the saturated magnetization (M_s). Numbers in the round brackets represent the order of the measurements. The first and third M–H

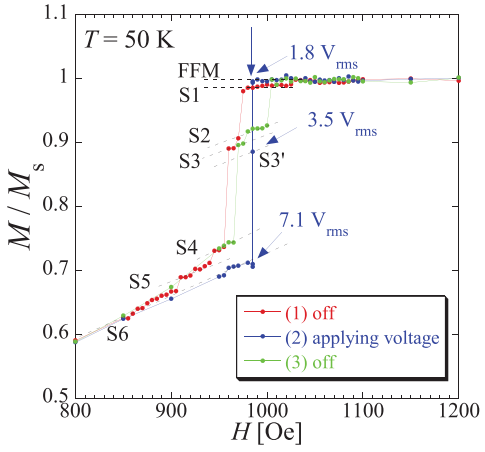

FIG. 2. M–H curves at 50 K during the H-decreasing process. The given number is the order of the measurements. S1–S6 show different states of the CSL estimated based on discrete changes in M. The first and third measurements were conducted without applying V. The blue arrows indicate H when V was applied.

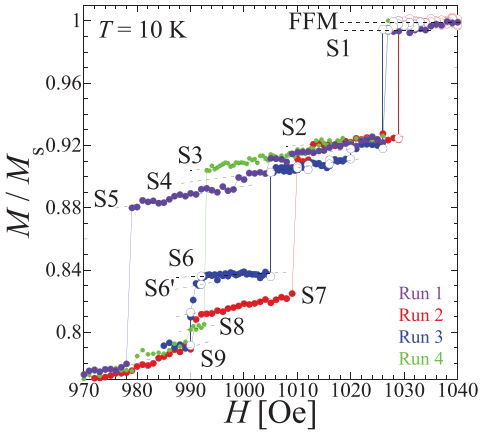

FIG. 3. *M–H* curves at 10 K in the *H*-decreasing process. S1–S9 show different states of the CSL estimated based on discrete changes in *M*. The open symbols indicate the *H* accompanying *V* application. The first and fourth runs were measured without applying *V*. In the second run, the measurement was performed by applying pulses like *V* between 1040 Oe and 1029 Oe. In the third run, the measurement was performed by applying pulses like *V* at selected *H* between 1033 Oe and 990 Oe.

measurements were conducted before and after a measurement by applying *V* to the transducer, respectively. The states termed S1–S6 show six CSL states with different soliton numbers estimated based on discrete changes in *M*, and the states for $H > H_c$ and $H = 800$ Oe are FFM and S6, respectively. The S1 state was only observed in the first measurement, suggesting thermally activated soliton nucleation (not observed regularly). In the third run, the FFM state transformed to S2 without passing S1, whereas S3 and S4 appeared similar to those in the first run. The discrete change in *M* to the S2 state in the third run appears at a slightly higher *H* than its *H* value in the first run. This slight shift toward the higher *H* side is thought to originate from residual strain (see the supplementary material). In the second run, we applied pulse-like *V* at 985 Oe, which is 10 Oe higher than the *H* value for avalanche soliton nucleation of S1–S2 in the first run. The application time was approximately 300 ms. First, we applied an amplitude of 1.8 V_{rms}, but we could not change the FFM state to the CSL. Next, at the same *H*, we increased the amplitude of *V* to 3.5 V_{rms}. *M* dropped down from the FFM state to the additional state S3′, which was not observed without *V* application. This discrete change in *M* nearly corresponds to the nucleation of 24 solitons per chiral chain. Furthermore, when we increased the amplitude up to 7.1 V_{rms}, we controlled the CSL state from S3′ to S6, which nearly corresponds to the nucleation of 36 solitons per chiral chain, without passing S4 and S5.

The effects of the surface barrier become more prominent at lower temperatures. We could control more changes in the soliton number of the CSL state in a further stepwise manner. Figure 3 shows *M* during the *H*-decreasing process from 2000 Oe ($>H_c$) at 10 K. The first run was measured without applying a pulse-like *V*. Here, S1–S9 represent the CSL state observed at $T = 10$ K through four runs. The first run followed the sequence as FFM → S1 (at 1034 Oe) → S2 → S3 → S4 → S5 → S9. The discrete changes in *M* for S1–S2 and S5–S9 are prominent. The S1 state in the first run corresponds to S1 in Fig. 2. The second run was performed by applying a pulse-like *V* between 1040 and 1029 Oe in intervals of 1 Oe, indicated by open symbols. We applied *V* with an amplitude of 5.4 V_{rms} up to seven times for each *H*. First, we applied *V* for 2.4 μs and then extended the application time up to 240 ms whenever a discrete change could not be observed. After changing the application time and measuring, we changed to the next *H*. The details of the application time for second and third runs are given in the supplementary material. Discrete changes were not observed even when *V* was applied for 240 ms at 1030 Oe. The FFM state changed to the CSL state when *V* was applied for 24 μs at 1029 Oe. We did not apply *V* below 1028 Oe. The second run followed the sequence FFM → S2 → S4 → S7 → S9. The third run was performed by applying a pulse-like *V* between 1033 and 990 Oe. The open symbols indicate *H* accompanying the *V* application in the third run (1033–1026 Oe in intervals of 1, 1020, 1016, 1012, 1010, 1005, 992, and 990 Oe). We applied *V* with the amplitude of 5.4 V_{rms}. The maximum time of the *V* application was 240 ms. We observed the S1 state immediately after stabilizing $H = 1027$ Oe, and any change did not observed with dynamic strain. The S1 state changed to the S2 state when *V* was applied for 24 μs at 1026 Oe. The third run followed the sequence FFM → S1 → S3 → S4 → S6 → S6′ → S7 → S9. After three runs, we measured the fourth run without applying *V*. The fourth run followed the sequence as FFM → S2 → S3 → S8 → S9. We note that the FFM state transformed to the CSL state at the same *H* within an error of ±5 Oe whether dynamic strain was applied or not. We assumed that the residual strain affected subsequent avalanche soliton nucleation in this case. Comparing the four measurements, additional states (S6, S6′, and S7) were observed when dynamic strain was applied to the CSL state. Thus, preparing various manners of applying dynamic strain, we can artificially realize CSL states, which are not stabilized in conditions without dynamic strain. In order to realize arbitrary CSL states, we must prepare a more detailed prescription.

Finally, note that the aforementioned results do not originate from the heating effect. We applied the voltage to the transducers with an amplitude of at most 7.1 V_{rms} and an application time of at most 300 ms. The transducer has a cross section of 4×3 mm^2, which is two hundred times larger than that of the $CrNb_3S_6$ crystal and is coated with gold, as shown in Fig. 1(d). Therefore, heating effects could not be detected using a thermometer and are considered to be almost negligible. Figure 4 shows the temperature (*T*) dependence of magnetization, *M–T* curve, which is compared with the *M–H* curve of the second run shown in Fig. 2. The *M–T* curve was measured according to the following sequence: First, we let *T* settle at 50 K from well above T_c in the mode of zero-field cooling. Next, we applied an *H* value of 2000 Oe and decreased it to 985 Oe. The intervals of *H* were 50 Oe between 2000 and 1100 Oe and 5 Oe between 1100 and 985 Oe. Then, we measured the *M–T* curve at an *H* value of 985 Oe in the sequence of 50 → 120 → 50 K. This situation was equivalent to a measurement for inducing the transformation from FFM to any CSL state by thermal energy in the vicinity of *H* appropriate for vanishing the surface barrier (with an error of ± 25 Oe). Many discrete changes in *M* were observed, for instance, at 55, 70, 72, 83 K, etc., and the magnitude of discreteness decreases with increasing *T*. By settling a certain state just before avalanche soliton nucleation as a starting state, we can realize the avalanche soliton nucleation by yielding thermal energy. The black dotted line is given as a guide to the eye to assume the increase in *T* from 50 K to 80 K and then measure *M* decreasing *T* down to 50 K again. For explaining the change from FFM to S3′ in Fig. 2 while ignoring the dynamic strain and considering only the heat

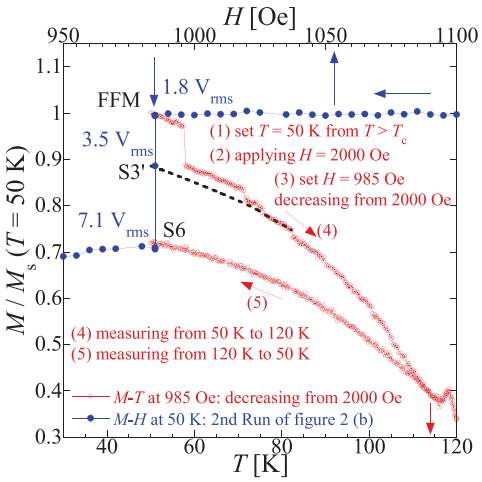

FIG. 4. Comparison of the *M–T* curve and the *M–H* curve. Blue plots show the *M–H* curve at 50 K (second run in Fig. 2). Red plots show the *M–T* curve at 985 Oe. The black dotted line is given as a guide to the eye if we increase *T* from 50 K to 80 K, with the subsequent decrease to 50 K.

contribution, we need to rapidly increase *T* up to 80 K. As for the change from S3′ to S6, we need to rapidly increase the *T* to 110 K or more. Because it is impossible for the temperature to increase rapidly from 50 to 110 K only due to heating by applying pulse-like acoustic waves using the transducer, it is considered that the observed phenomena in Figs. 2 and 3 originate from the modification of the surface barrier due to dynamic strain.

In conclusion, we controlled the number of solitons of the CSL and transformed the magnetic configuration from the FFM state to the CSL state by measuring *M–H* curves of a thin single crystal of $CrNb_3S_6$ using dynamic strain. We changed the magnetic configuration from the FFM state to the CSL state and the number of solitons of the CSL by the acoustic wave with pulse widths of 30 μs and 300 ms, respectively. A dynamic structural modification and a static one are useful methods for manipulating spin systems in monoaxial chiral magnets.

Magnetoelastic resonance in a monoaxial chiral magnet had been studied before.[24] In a forced magnetic state with *H* parallel to the helical axis, the linearly polarized elastic wave can be converted to a circularly polarized wave with chirality opposite to the spin-wave chirality.

Surface acoustic wave application along or perpendicular to the chiral axis is also a very interesting situation. Nucleation of magnetic skyrmions in the multilayer films by surface acoustic waves has been investigated.[25] Further experimental studies of magnetoelastic coupling on a monoaxial chiral magnet may provide a wealth of promising applications.

See the supplementary material for measurements of *M–H* curves at 10 K with dynamic strain and a detailed description of the application time of dynamic strain.

We acknowledge Mr. K. Takahashi (Asahi International Techno Co. Ltd.) for help in crystal machining. This work was supported by the Grants-in-Aid for Scientific Research, Grant No. (S) 25220803, from the Ministry of Education, Culture, Sports, Science and Technology (MEXT), Japan. This work was also supported by the Center for Chiral Science in Hiroshima University (the MEXT program for promoting the enhancement of research universities, Japan) and JSPS Core-to-Core Program, A. Advanced Research Networks.

DATA AVAILABILITY

The data that support the findings of this study are available from the corresponding author upon reasonable request.

REFERENCES

[1]I. E. Dzyaloshinskii, J. Phys. Chem. Solid **4**, 241 (1958).
[2]T. Moriya, Phys. Rev. **120**, 91 (1960).
[3]Y. Togawa, Y. Kousaka, S. Nishihara, K. Inoue, J. Akimitsu, A. S. Ovchinnikov, and J. Kishine, Phys. Rev. Lett. **111**, 197204 (2013).
[4]J.-I. Kishine and A. Ovchinnikov, Solid State Phys. **66**, 1 (2015).
[5]M. Mito, H. Ohsumi, K. Tsuruta, Y. Kotani, T. Nakamura, Y. Togawa, M. Shinozaki, Y. Kato, J.-I. Kishine, J.-I. Ohe *et al.*, Phys. Rev. B **97**, 024408 (2018).
[6]M. Shinozaki, Y. Masaki, R. Aoki, Y. Togawa, and Y. Kato, Phys. Rev. B **97**, 214413 (2018).
[7]Y. Togawa, T. Koyama, K. Takayanagi, S. Mori, Y. Kousaka, J. Akimitsu, S. Nishihara, K. Inoue, A. S. Ovchinnikov, and J. Kishine, Phys. Rev. Lett. **108**, 107202 (2012).
[8]T. Miyadai, K. Kikuchi, H. Kondo, S. Sakka, M. Arai, and Y. Ishikawa, J. Phys. Soc. Jpn. **52**, 1394 (1983).
[9]Y. Togawa, T. Koyama, Y. Nishimori, Y. Matsumoto, S. McVitie, D. McGrouther, R. L. Stamps, Y. Kousaka, J. Akimitsu, S. Nishihara *et al.*, Phys. Rev. B **92**, 220412 (2015).
[10]K. Tsuruta, M. Mito, Y. Kousaka, J. Akimitsu, J-i Kishine, Y. Togawa, H. Ohsumi, and K. Inoue, J. Phys. Soc. Jpn. **85**, 013707 (2016).
[11]K. Tsuruta, M. Mito, Y. Kousaka, J. Akimitsu, J. Kishine, Y. Togawa, and K. Inoue, J. Appl. Phys. **120**, 143901 (2016).
[12]L. Wang, N. Chepiga, D.-K. Ki, L. Li, F. Li, W. Zhu, Y. Kato, O. S. Ovchinnikova, F. Mila, I. Martin *et al.*, Phys. Rev. Lett. **118**, 257203 (2017).
[13]J.-I. Yonemura, Y. Shimamoto, T. Kida, D. Yoshizawa, Y. Kousaka, S. Nishihara, F. J. T. Goncalves, J. Akimitsu, K. Inoue, M. Hagiwara *et al.*, Phys. Rev. B **96**, 184423 (2017).
[14]M. Ohkuma, M. Mito, N. Nakamura, K. Tsuruta, J. Ohe, M. Shinozaki, Y. Kato, J. Kishine, Y. Kousaka, J. Akimitsu *et al.*, AIP Adv. **9**, 075212 (2019).
[15]M. N. Wilson, E. A. Karhu, D. P. Lake, A. S. Quigley, S. Meynell, A. N. Bogdanov, H. Fritzsche, U. K. Rößler, and T. L. Monchesky, Phys. Rev. B **88**, 214420 (2013).
[16]S. A. Meynell, M. N. Wilson, H. Fritzsche, A. N. Bogdanov, and T. L. Monchesky, Phys. Rev. B **90**, 014406 (2014).
[17]J. Müller, A. Rosch, and M. Garst, New J. Phys. **18**, 065006 (2016).
[18]A. O. Leonov and K. Inoue, Phys. Rev. B **98**, 054404 (2018).
[19]M. Mito, T. Tajiri, K. Tsuruta, H. Deguchi, J. Kishine, K. Inoue, Y. Kousaka, Y. Nakao, and J. Akimitsu, J. Appl. Phys. **117**, 183904 (2015).
[20]G. W. Paterson, A. A. Tereshchenko, S. Nakayama, Y. Kousaka, J. Kishine, S. McVitie, A. S. Ovchinnikov, I. Proskurin, and Y. Togawa, Phys. Rev. B **101**, 184424 (2020).
[21]T. Tajiri, M. Mito, Y. Kousaka, J. Akimitsu, J-i Kishine, and K. Inoue, Phys. Rev. B **102**, 014446 (2020).
[22]K. Tsuruta, M. Mito, Y. Togawa, Y. Kousaka, J. Akimitsu, and K. Inoue, J. Phys.: Conf. Ser. **969**, 012132 (2018).
[23]Y. Kousaka, Y. Nakao, J. Kishine, M. Akita, K. Inoue, and J. Akimitsu, Nucl. Instrum. Methods Phys. Res., Sect. A **600**, 250 (2009).
[24]A. A. Tereshchenko, A. S. Ovchinnikov, I. Proskurin, E. V. Sinitsyn, and J.-I. Kishine, Phys. Rev. B **97**, 184303 (2018).
[25]T. Yokouchi, S. Sugimoto, B. Rana, S. Seki, N. Ogawa, S. Kasai, and Y. Otani, Nat. Nanotechnol. **15**, 361 (2020).